# Nestos River plume dynamics under variable physical forcing

Kamidis N.[1], Sylaios G.[2] & Tsihrintzis V.A.[3]
[1] NAGREF - Fisheries Research Institute, Nea Peramos, 64007 Kavala, Greece, nikkami@inale.gr
[2] Democritus University of Thrace, Department of Environmental Engineering, Laboratory of Ecological Engineering and Technology, 67100 Xanthi, Greece, gsylaios@env.duth.gr
[3] National Technical University of Athens, School of Rural and Surveying Engineering, Department of Infrastructure and Rural Development, Laboratory of Reclamation Works and Water Resources Management, 9 Iroon Polytechniou St., Zografou 157 73 Athens, Greece, tsihrin@central.ntua.gr

**Abstract**
The three-dimensional numerical model ELCOM was utilized to quantify the degree of influence of each physical forcing upon Nestos River plume. The model was calibrated and validated by a significant number of field samplings, collected during years 2006-2007. After the successful implementation and validation of the model, a series of scenarios were devised, isolating the impact of each physical force, such as wind speed and direction, tidal range, river discharge and coastal morphology. Further scenarios combined or altered forcing factors, aiming to distinguish the forces that play a primary role upon the plume dynamics. Results showed that Nestos River plume is mainly wind-driven, while its size depends on river discharge. The plume follows the direction of the wind having a small clockwise deflection. The wind speed is an important factor as it pushes the plume away from the mouth, while elevated wind speed enhances vertical mixing with the ambient water. Under low wind conditions, the Coriolis force becomes more dominant. Due to its narrowing, Thassos Passage also plays a special role on the western expansion and plume's shape and evolution. Surface waters within this strait gain extra speed and under high river discharge the plume enters Kavala Gulf. Tide has only a minor role on plume's evolution due to the micro-tidal nature of the area.

**Keywords:** Nestos River, river plume, Thracian Sea, coastal zone, hydrodynamic model, physical forcing

## Introduction

River plumes are created by the continuous freshwater discharge into coastal seas, while the principal parameter of their formation is the density difference between these two water bodies (Garvine 1974). Plumes are acting as intermediate bodies and under certain circumstances they are able to 'carry' the river water characteristics at long distance from the mouth (Gaston et al. 2006). The recognition of river plume importance during the last decades has led many scientists to the need of understanding the plume dynamics, with the use of mathematical models. Chao and Boicourt (1986) were the first to study the structure of plumes and the generated alongshore current by using a three-dimensional hydrodynamic model incorporating non-linear turbulent mixing. Among many others, the wind influence was studied by Chao (1988). Xing and Davies (1999) showed that wind shear stress enhances vertical mixing, thus affecting the vertical and horizontal plume structure. Coriolis force influence was examined by Garvine (1981, 1982), while the alternation of plume's behavior due to coastline morphology was studied by Wiseman and Garvine (1995). The importance of the tide was highlighted by Chao (1988) and Kourafalou et al. (1996a, b). Under specific conditions, the plume can be pushed back or released at the mouth area depending on the tidal cycle (Hetland and MacDonald 2008; MacCready et al. 2009), promoting in this way the vertical mixing of the plume and delaying its horizontal spreading.
Based on these model results several classification schemes have been proposed in order to categorize plumes according to their shape and size. Depending on the river discharge and latitude, Garvine (1995) classified river discharge as "large" and "small" scale with the introduction of Kelvin number ($K$). When $K < 1$, the discharge is considered as "small", the formed plume is unstable and dissolved before being given the chance to deflect clockwise by the Earth's rotation. On the other hand, if $K > 1$ then the discharge is characterized as "large-scale" and the plume's shape is significantly affected by Coriolis force. Another classification

parameter is the Froude number (*Fr*) which is based on the plume's speed ($u_p$) and the gravitational wave speed (*c*, Garvine 1987). According to Chao (1988) and Kourafalou et al. (1996a, b), when *Fr*< 1 the freshwater bulge size at the mouth is comparable with the width of the alongshore current and the plume is "subcritical". If *Fr*> 1 then the anticyclonic gyre at the mouth gains a considerable size and the coastal current width is smaller. The bulge tends to hold and spin increasing amount of freshwater and the mixing with the ambient water is limited. In this case, the plume is classified as "supercritical".
In this work, the evolution of Nestos River plume is studied under different and variable physical forcing, with the use of ELCOM hydrodynamic model. The successful calibration and validation of the model by a significant number of field campaigns, presented an opportunity to study the plume's behavior by isolating or alternating a variety of physical parameters, such as wind speed and direction, river discharge, tidal range and coastal morphology, in order to identify and comprehend the forces that play a major role upon the plume shape and expansion.

**Materials and Methods**

*Study Area Description*

Nestos River has its source in Rila Mountains (southwestern Bulgaria), draining an area of approximately 5,600 km², of which 2,800 $km^2$ belong to Greece (Ganoulis et al. 2008; Kamidis et al. 2011) and has a total length of 230 km (Petalas et al. 2005; Boskidis et al. 2012). Nestos natural flow is interrupted by the construction and operation of two dams in the Greek part, at the sites of Thisavros and Platanovrisi during late 1990s. A third dam at Toxotes site was constructed during the 1960s in order to re-distribute the river water to the downstream irrigation network for the 131 $km^2$ arable land of the deltaic zone.
According to the Public Electricity Cooperation (DEI) data, the mean pre-damming annual discharge during the period 1966-1996 was 39.7 $m^3/s$, characterized by a strong seasonal and inter-annual variability (Ganoulis et al. 2008). Concerning Nestos discharge, Koutroumanidis et al. (2009) divided the above pre-damming period into 5 different hydro-periods, at which the mean annual flow appears continuously decreased. The most recent hyrdo-period (1986-2004), presented a reduced mean annual flow by 51.2 % compared to the 1966-1971 hydro-period.
Nestos River outflows NE of Thassos Island, between Kavala and Vistonikos Gulf (Fig. 1) into the Thracian Sea. The main feature of Thracian Sea is the wide continental shelf, reaching at 65 km south of Samothraki (Isari et al. 2008). At the vicinity of the River mouth, the bathymetry gradually increases up to 50 m depth on the east of Thassos Island. Nestos mouth is at the eastern boundary of Thassos Passage, a natural channel 13 km long, 7.3 km wide and 25 m deep, which narrows the alongshore circulation before its entry to Kavala Gulf (Sylaios et al. 2013). The investigated area is under the influence of the less saline (32-35) and colder (20-22 $^oC$) Black Sea Water (BSW), discharged through the Dardanelles Strait and moving cyclonically along the Thracian Sea coastline (Yüce 1995; Lykousis et al. 2002; Sylaios et al. 2005). BSW occupies the first 40 m of the water column, overtopping the more saline and warmer Levantine Intermediate Water (LIW; Poulos et al. 1997).

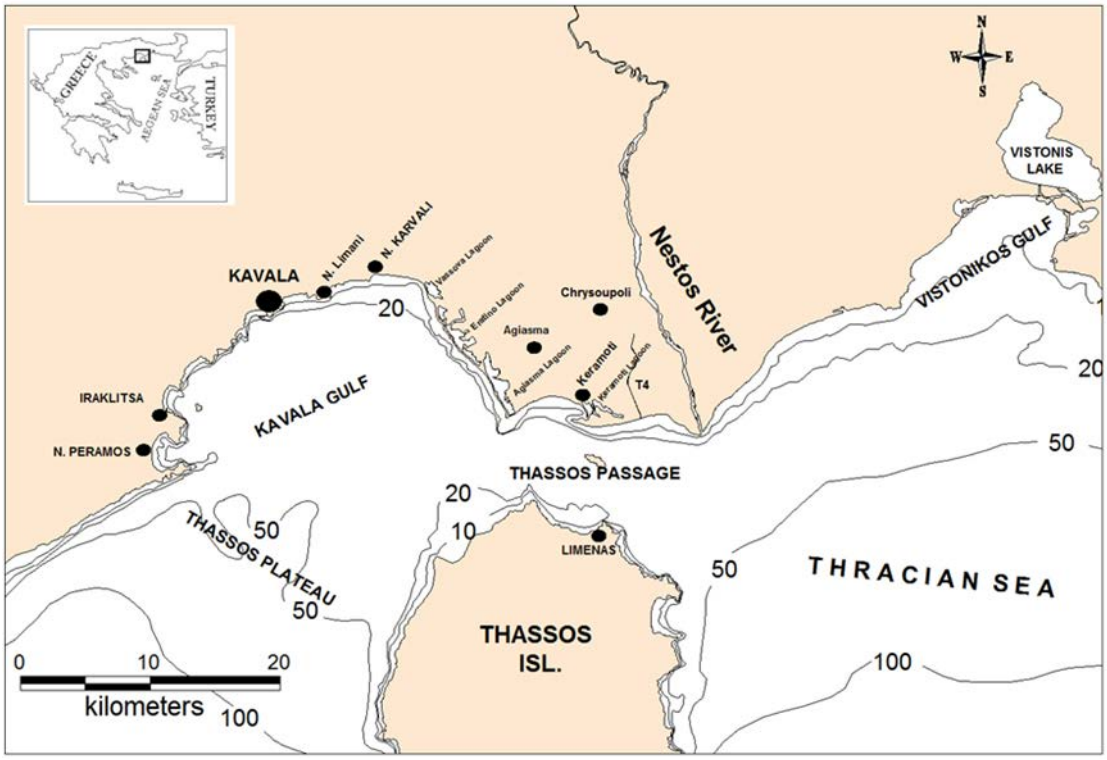

Figure 1. Wider area of Nestos freshwater influence.

*Model Description, Implementation and Calibration*

The simulation of Nestos River plume was achieved using the Estuary and Lake Computer Model (ELCOM), a three-dimensional hydrodynamic model developed by the Centre for Water Research (CWR, Hodges 2000; Hodges and Dallimore 2006). ELCOM is used to simulate the variation of salinity and temperature in space and time for estuaries, lakes and reservoirs by solving the unsteady, 3D-Reynolds averaged, hydrostatic, Navier-Stokes, Bussinesq equations and the scalar transport equations for salinity, temperature, tracers, and incorporating a mixing model for vertical turbulent transport (Laval et al. 2003). The unsteady Reynolds-averaged equations were solved on an Arakawa C-grid using a semi-implicit method with quadratic Euler–Lagrange discretization of momentum advection (Casulli and Cheng 1992), while a conservative ULTIMATE QUICKEST approach was used for scalar transport (Leonard 1991; Romero et al. 2004).

The modeled area covered the broader Nestos River shelf, discretized into a uniform horizontal grid consisting of 89×53 orthogonal cells (4,717 in total) with 1 × 1 km size. A maximum number of 59 variable in thickness layers were used to discretize the water column in each horizontal cell. Surface layers were thinner (0.5 m), with thickness increasing gradually towards the bottom layers, reaching 20 m. The calibration procedure included model runs under several combinations of bottom drag coefficient ($C_D$) and horizontal eddy diffusivity values ($k_{1,2}$), in order to achieve the best possible salinity simulation. The validity of model calibration was statistically tested over the entire water column ($N$ = 225 cases) for a high river flow incident (March 2006), under which the river plume was more evident. The accuracy of each model output was tested using various statistical criteria, such as the squared-correlation coefficient $R^2$, the slope of the linear regression line $\gamma$ fitted between observed and predicted data, the root-mean-squared-error *RMSE* and the scatter index *SI*. Detailed information regarding the model calibration can be found in Kamidis et al. (2011).

*Data Collection and Model Validation*

The validity of the model was tested by carrying out 12 coastal samplings during the period 2006 -2007 in a number of stations as shown in Figure 2. At these stations, salinity values

were recorded in the entire water column with the use of a SBE 19plus CTD. The comparison between measured and predicted data from all samplings was achieved using the statistical criteria mentioned above and presented in Table 1. Initial conditions in terms of salinity were defined at the grid domain based on the November 2005 survey. Nestos discharge and salinity values were measured through an auto-recording telemetric station, located 20 km upstream of the river mouth. The station is equipped with an acoustic current-meter and conductivity sensors. The measurements were recorded at a 1-hr interval. The above data were used to define the boundary condition of the model, in the form of river discharge time-series. Tidal forcing at the open boundaries was determined by applying the basic semi-diurnal $M_2$ and diurnal $S_1$ tidal constituents, with amplitudes 0.20 and 0.15 m and phases 32.9 and 350.5 degrees, respectively (Sylaios et al. 2008). Meteorologic forcing, such as solar radiation intensity, atmospheric temperature, atmospheric relative humidity, precipitation, wind speed and wind direction were acquired from NOAA database (http://ready.arl.noaa.gov/READYamet.php) and applied to the simulated area with 3-hrs interval.

Table 1. ELCOM model efficiency regarding salinity prediction, based on the statistical criteria considered.

| **Months** | ***n*** | ***$R^2$*** | ***γ*** | ***RMSE*** | ***SI(%)*** |
|---|---|---|---|---|---|
| March 2006 | 225 | 0.886 | 1.011 | 1.061 | 3.00 |
| May 2006 | 337 | 0.635 | 1.039 | 2.159 | 6.24 |
| August 2006 | 230 | 0.807 | 1.054 | 2.317 | 6.60 |
| October 2006 | 230 | 0.830 | 1.030 | 1.217 | 3.45 |
| November 2006 | 384 | 0.764 | 1.013 | 0.583 | 1.59 |
| January 2007 | 391 | 0.614 | 1.008 | 0.518 | 1.40 |
| February 2007 | 449 | 0.446 | 1.001 | 0.319 | 0.86 |
| April 2007 | 420 | 0.604 | 1.006 | 0.424 | 1.15 |
| May 2007 | 355 | 0.678 | 1.017 | 0.831 | 2.31 |
| August 2007 | 296 | 0.833 | 1.036 | 1.498 | 4.19 |
| September 2007 | 364 | 0.650 | 1.030 | 1.251 | 3.52 |
| November 2007 | 251 | 0.690 | 0.996 | 0.364 | 0.98 |

To reveal the influence of external factors upon Nestos plume behavior, a series of different simulation runs were set and their settings are presented in detail in Table 2. At all cases the surface salinity was set to 33, increasing gradually in depth, simulating a water column identical to winter period. The plume evolution was examined by varying physical forces such as wind speed, wind direction, tidal range, river discharge, as well as by altering the coastal morphology of the area by removing Thassos Island. Five points were defined to study the temporal fluctuations in the salinity and hydrodynamic fields, the location of which is presented in Figure 3.

Table 2. Parameters settings chosen for the modeled cases, used for Nestos plume examination

| **Simulation Run** | **Discharge ($m^3/s$)** | **Wind** | | **Notes** |
|---|---|---|---|---|
| | | **Speed (m/s)** | **degrees (°)** | |
| R1 (Reference) | 40 | 0 | - | only Coriolis force was applied |
| R2 | 40 | 0 | - | tidal range was introduced to the open boundaries together with Coriolis |
| R3 | 40 | 2 m/s | 45 | similar to R2 case, testing the influence of northeastern wind |
| R4 | 40 | 2 m/s | 225 | similar to R2 case, testing the influence of southwestern wind |
| R5 | 40 | 2 m/s | 90 | similar to R2 case, testing the influence of eastern wind |
| R6 | 40 | 4 m/s | 90 | similar to R2 case, testing the influence of wind speed |
| R7 | 80 | 2 m/s | 90 | similar to R2 case, testing the influence of elevated discharge |
| R8 | 40 | 2 m/s | 0 | similar to R2 case, testing the influence of northern wind |
| R9 | 40 | 2 m/s | 0 | similar to R2 case, testing the plume evolution by eliminating Thassos Passage |

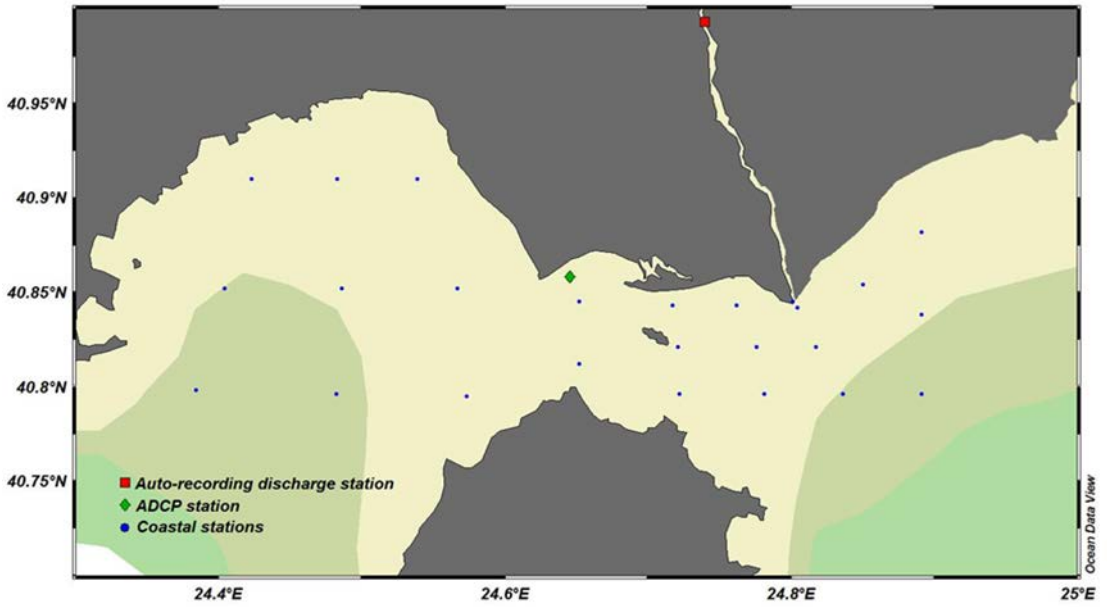


Figure 2. Location of sampling sites along the coastal zone. The map also shows the site of the automated station used for discharge measurement.

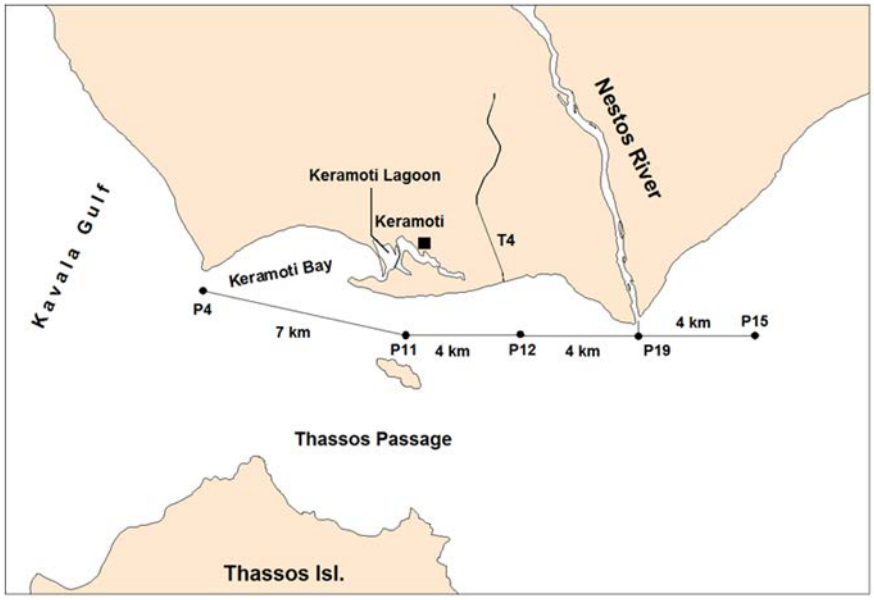


Figure 3. Location of check points used for the representation of salinity, horizontal and vertical velocities fluctuations derived from ELCOM model.

**Results and Discussion**

*Tidal range influence*

The investigation of the tidal influence on the behavior of Nestos plume was achieved through two simulation runs: the first (R1) in which only the Coriolis force was applied (Reference case) and at the second (R2), in which the tidal range was introduced from all open boundaries together with Coriolis. In both cases river discharge was set at 40 $m^3/s$ (representing an occurrence frequency of 20.3% for year 2006), while to eliminate the atmospheric influence no wind was considered. The variation of salinity, surface elevation and vertical velocity (*w)* was calculated by the model at points P11 (Thassos Passage) and P19 (Nestos mouth) with an hourly interval. On day 3 the plume was fully developed and

showed similar shape for both cases (Fig. 4a and 4b), suggesting no influence from tide introduction. As expected, an anticyclonic eddy was formed at the mouth, due to the Coriolis force, followed by a downstream current which transports freshwater to the west (Kourafalou 1996a, b; Fong 1998). Under this specific discharge, the anticyclone was formed at $T$ = 9 hours, and 5 hours later a coastal current was developed having a width of 2 - 3 km. The temporal variation of salinity for the case R2 at point P11 revealed some minor differences compared to simulation R1 (Coriolis only). The plume arrived at point P11 after $T$ = 30 hours from model start, having 6 hours delay in relation to R1 simulation (Fig. 4c). By the time $T$ = 90 hours, surface salinity in the R2 case ranged at higher levels, but the difference is negligible compared to R1 simulation (mean difference: 0.11 psu). By the time $T$= 95 hours, salinity values in both scenarios were almost identical.

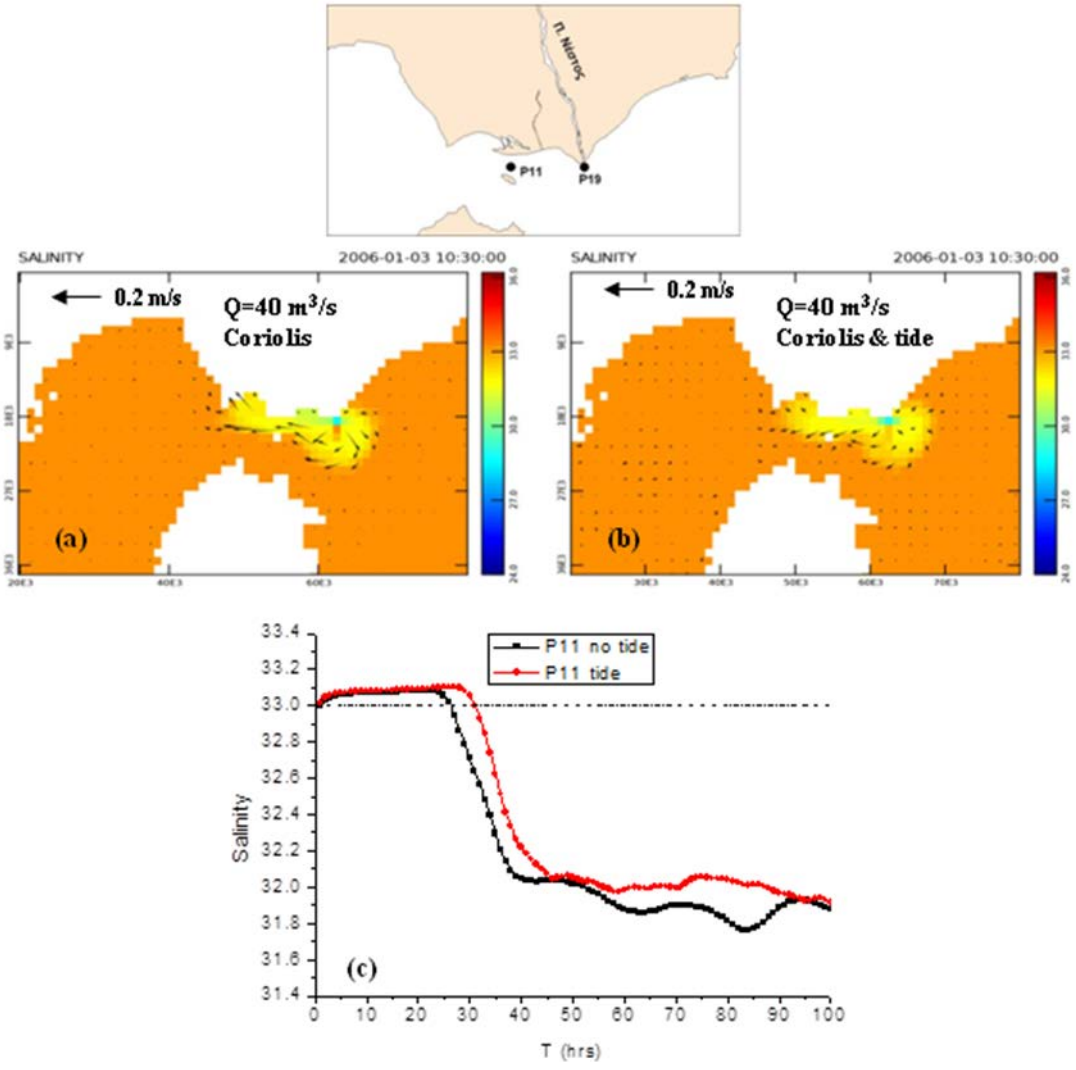


Figure 4. Surface salinity distribution during the 3rd day of the simulation: (a) R1 (Coriolis only) and (b) R2 with the introduction of tidal range. The temporal fluctuation of salinity at P11 point is illustrated in (c).

The tidal influence was examined in more details at point P19 (Fig. 5). From the simulation results, it is apparent that salinity values at the mouth depend on the tidal phase. Higher salinity is associated with tidal flood (Fig. 5a), at which the freshwater was pushed towards the mouth, while lower salinity with the tidal ebb , at which the released water resulted to a salinity decrease of 2.5, compared to the R1 case, for the same time period (Fig. 5b). Similar behavior was reported in other studies related to the tidal influence on plumes (Liu et al.

2000; Bricker et al. 2006). At the mouth, the introduction of the tidal range resulted to the enhanced mixing of the plume with the underlying layers, due to vertical velocity (*w*) increase (Fig. 5c). Comparing the peaks of salinity and vertical velocity *w* in Figure 5c, it is concluded that the reaction of the plume to tidal range varies by about three hours. During the third day of the R2 simulation, the plume occupied the first 4 m of the water column, while in the simulation R1 plume's thickness was found at 3 m. Higher vertical mixing explains the intensive dilution of the plume in the case of these tidal range scenarios. Nevertheless, the characteristics of the two plumes were almost identical. As reported by Mestres et al. (2003) and Ulses et al. (2005), a Mediterranean feature, such as the small tidal range, does not cause major changes on plume's behavior. As a result, the offshore spreading was found at 6 km in both cases. The Froude number was calculated to be at 0.3 and 0.12, for the R1 and R2 simulations, respectively, so the plume is subcritical in both occasions. The Kelvin number was measured at 2.6 and 2.4, respectively, indicating the predominance of Coriolis force.

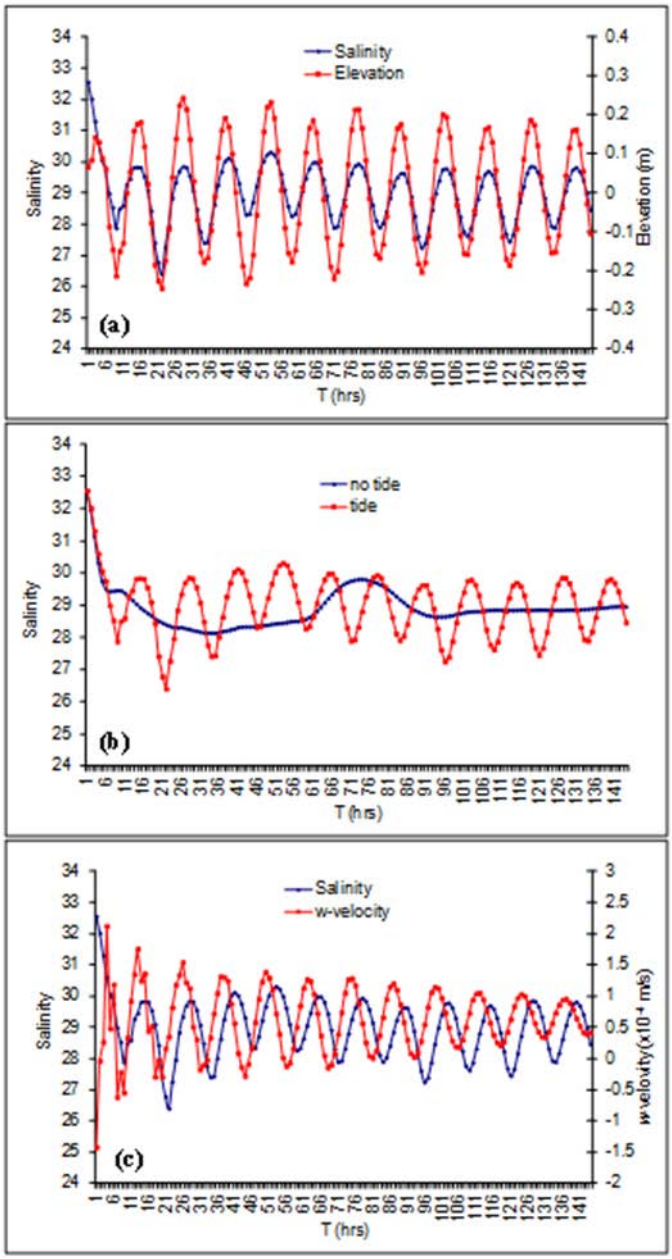


Figure 5. Temporal distribution of: (a) salinity in accordance to surface elevation for R2 case, (b) surface salinity during R1 and R2 cases at P19 and (c) vertical velocity w together with surface elevation of R2 case at P19 checkpoint.

*Wind direction influence (NE)*

The wind influence was investigated with the introduction of NE wind (case R3). The wind speed was set at 2 m/s (representing occurrence of 17.1% and 21.4% for years 2006 and 2007, respectively) and river discharge at 40 $m^3$/s. Coriolis force and tidal forcing were also applied. The plume evolution was examined at P4 and P11 (Fig. 6). Under the influence of northeastern wind (36% of occurrence), the plume headed westwards due to Ekman transport (Horner-Devine et al. 2009; MacCready et al. 2009) and arrived at the entrance of Kavala Gulf (P4 point) within $T$ = 1.1 days, half of the time needed during the R2 scenario. Point P4 continued to receive the plume water, which drastically reduced salinity up to $T$ = 11 days (32.1 psu). Beyond that point a relative balance is observed and salinity increased slightly to 32.3 until the end of the simulation (Fig. 6a). As for point P11, the plume arrived there at $T$ = 0.75 days. Salinity fluctuated considerably, and although point P11 is 7 km closer to the mouth, the mean surface salinity from the time of the plume arrival and by the end of the simulation was found similar to that in point P4 (32.3 psu). This is because this station is more exposed, due to its location, characterized by higher horizontal and vertical velocities (Fig. 6b and 6c). The extra energy provided by the wind increases the mixing of the plume with the underlying ambient water (Kourafalou et al. 1996a). The morphological characteristic of the plume and its evolution over time is presented in Figure 7. The introduced wind decreases the width of the anticyclone at the mouth which tends to disappear. The offshore spreading was found at 5 km, while the Froude number was estimated at 0.7, indicating that the plume remained subcritical, but it tends to become supercritical compared to R2 simulation. The Kelvin number was estimated at 1.7, which means that the effect of Coriolis remained significant. The plume entered Thassos Passage and moved in the form of a coastal current along the continental coastline (Fig. 7a). Because of the reduced width of the strait, the velocity of the surface layer reached 0.22 m/s during the third day, significantly higher than the speed of 0.07 m/s in the rest area. Due to this increased speed, the plume enters Kavala Gulf and follows the slope of the eastern coastline (Fig. 7b). Over time, the plume separates into two branches: the first branch moves along the coastline following the 20 m isobaths, while the second moves towards the center of Kavala Gulf (Fig. 7c), is diverted clockwise and forms an anticyclone. In this case the eastern entrance of the Gulf acted as a river mouth that outflows brackish water. The additional kinetic energy gained from the narrowing of Thassos Passage emulates the initial momentum of the river water at the mouth, while the first branch simulates the coastal current development. As the plume enters and moves towards the center of the Gulf, it is automatically converted into offshore current due to the northwestern slope of the shoreline. Further, another element that enhances the similarities between the Gulf's entrance and a river mouth is the gradually increase of depth from 26 m (entrance) to 42 m (center of the gulf). This situation therefore meets all the morphological and hydrodynamic criteria for an anticyclone development similar to those described by Kourafalou (2001) and Tanaka et al. (2009).

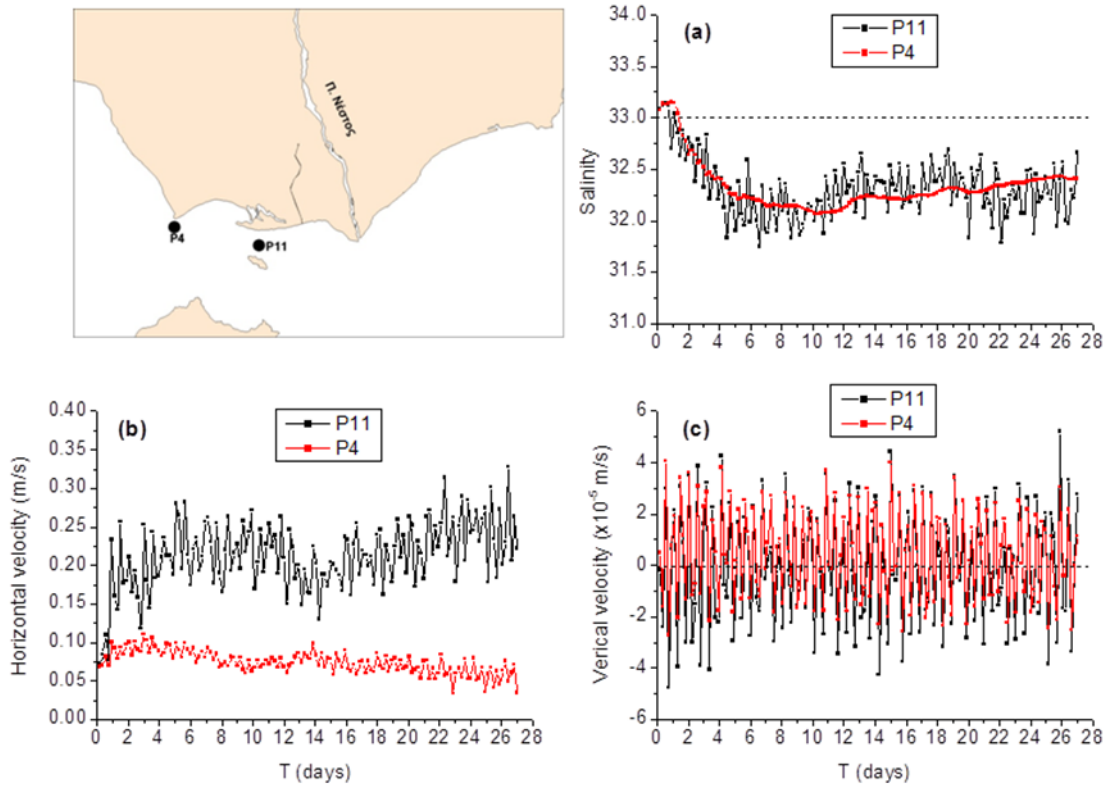


Figure 6. Temporal distribution of: (a) surface salinity, (b) horizontal velocity (positive values are indicating western movement) and (c) vertical velocity (negative values are indicating downward movement) at P4 and P11 checkpoints during the simulation R3.

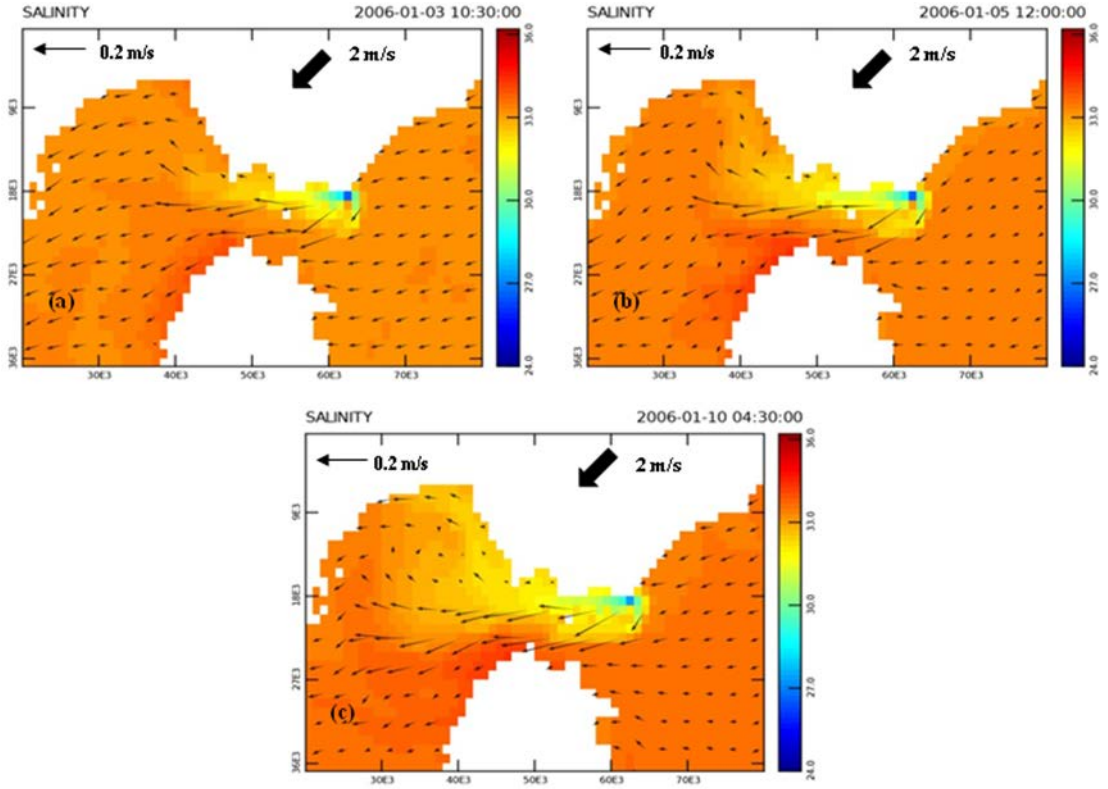


Figure 7. Nestos plume evolution with the introduction of 2 m/s NE wind during: (a) day 3, (b) day 5 and (c) day 10 of the simulation R3.

*Wind direction influence (SW)*

Southwesterly winds (210-250$^{o}$) at the investigated area exhibited an occurrence of 8.8 and 13.1% for the years 2006 and 2007, respectively. To examine the plume evolution, a simulation was carried out by applying a southwestern wind (225$^{o}$), while wind speed and river discharge were kept constant, as that in scenario R3. The plume evolution for this case (R4) was examined at point P15, located 4 km west of the mouth (Fig. 3). The comparison of salinity temporal variation at point 15 between R3 and R4 cases is presented at Figure 8. For R4 simulation, the point immediately receives the plume water and the salinity decreases to 32.3 psu. After $T$ = 2 days, the plume weakens significantly, but it is visible as the salinity ranges permanently below 33 psu, while during the R3 simulation no plume water reached that point, as the plume is headed to the west. Under constant SW wind the plume width at the mouth was simulated at 2.7 km. Froude number was measured to 0.4, thus remained subcritical. The baroclinic Rossby radius and Kelvin number were found at 2.1 km and 0.26, respectively, meaning that inertia prevailed over geostrophic forces.

Plume evolution during the R4 scenario is illustrated in Figure 9. During the third day, the freshwater from Nestos River moved eastwards, deflected clockwise by 45$^{o}$ from the wind direction due to Ekman transport. The velocity inside the plume was modeled ranging between 0.04 and 0.11 m/s. The wind direction opposes Coriolis force, and therefore, the anticyclone at the mouth was eliminated. On the fifth day, the plume continues to head east, but its path seems to be influenced by the general surface circulation. A surface current that moves eastwards through Thassos Passage entrained the plume at the same direction. The plume appeared to be weaker in comparison to the R3 scenario, because it is directed away from the coastline towards a deeper water column and it is more exposed. On day 10, the plume direction has changed to southeast, as the coastal current exiting the strait from the west became more stable.

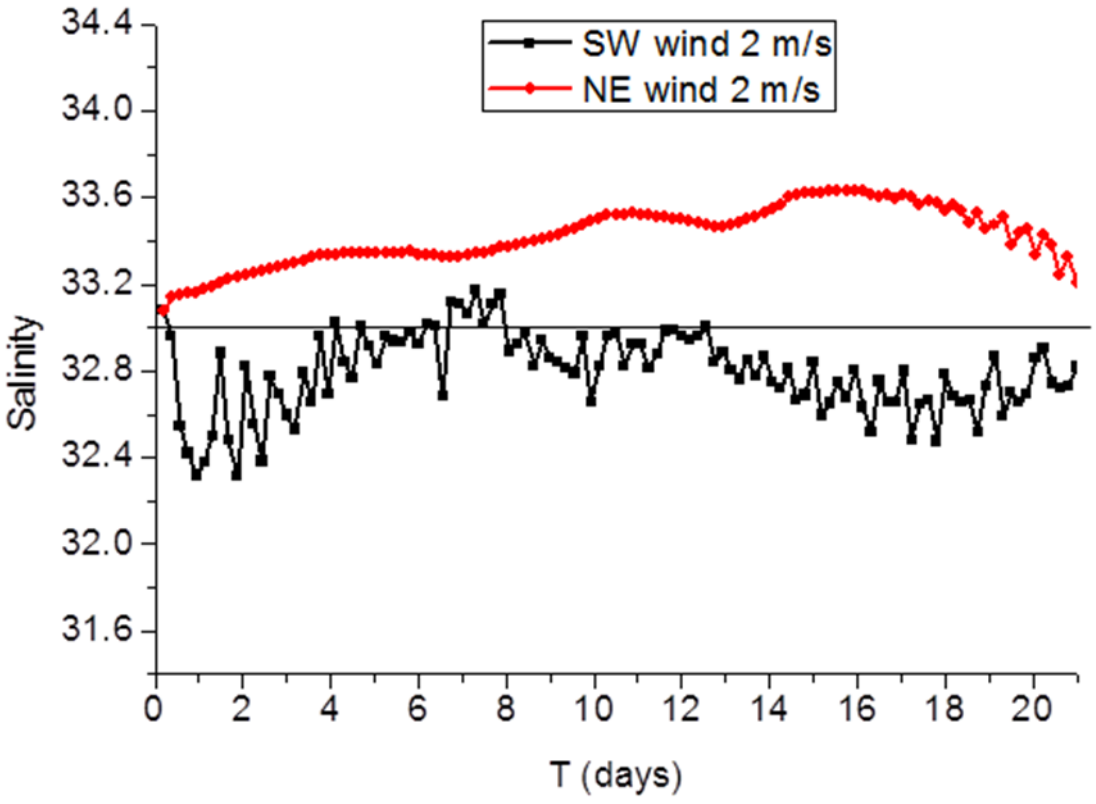


Figure 8. Temporal distribution of surface salinity at P15 for simulations R3 (NE wind) and R4 (SW wind).

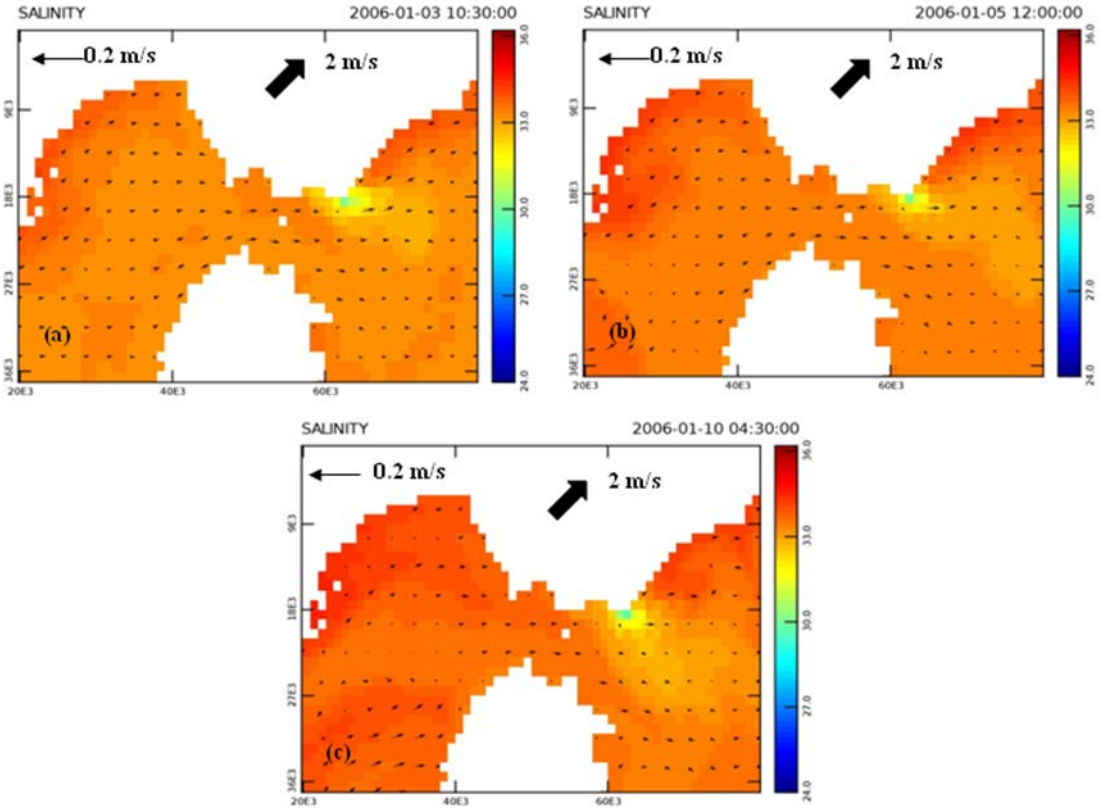

Figure 9. Nestos plume evolution with the introduction of 2 m/s SW wind during: (a) day 3, (b) day 5 and (c) day 10 of the simulation R4.

*Wind speed influence*

The examination of Nestos plume behavior by alternating wind speed was achieved with the introduction of easterly wind (8.4 and 6.6% in occurrence for 2006 and 2007, respectively) of 4 m/s (R6 case). The specific velocity was met at 16.5% of the cases for both years. The temporal variation of surface salinity is compared with the corresponding results at which the wind speed was kept at 2 m/s (R5 case). Nestos discharge was once again set to 40 $m^3$/s. The plume evolution for both cases is shown in Figure 10. For both simulations, the freshwater outflowing the mouth forms a well-defined plume, which is directed immediately westwards, due to the application of the eastern wind. The entry of the plume in Kavala Gulf occurred at $T$ = 1.8 days and $T$ = 1.5 days for R5 and R6 case, respectively. On the fifth day of simulation R5 (Fig. 10b), the plume is directed mainly northwestwards inside the Gulf, following a parallel course to the eastern coastline, while in R6 case the plume ejected towards the center of the gulf and deflected clockwise later. Under the influence of more intense wind, an anticyclone was formed on day 7, and carried part of the plume with it. The speed of the surface layer at the gulf's entrance was modeled at 0.38 m/s (0.2 m/s for case R5). On day 10, the plume in R5 case continued its path along the eastern and northern coastline of the Gulf and appeared more solid (Fig. 10c). Under 4 m/s wind, the anticyclone at the center of the Gulf is in its full development, and the plume forms two branches; the first is transmitted through the anticyclone and the second runs parallel to the coastline. In this case, the plume appears less visible. The additional kinetic energy gained by the extra wind speed enhances vertical mixing of the surface layer with the underlying seawater (Kourafalou et al. 1996a). The plume occupied the first 5 m and 9 m of the water column at the mouth for the R5 and R6 scenarios, respectively. For this reason, the surface coverage of the plume during the third day reached 63 $km^2$ (R5) and 45 $km^2$ (R6). Moreover, the two plumes showed different characteristics, demonstrating the significance of wind speed influence. In simulation R5, the plume is subcritical and its behavior is dominated by Coriolis ($Fr$ = 0.6, $K$ = 1.6), while in R6 case the plume turned to be supercritical with the prevalence of inertia ($Fr$ = 1.1, $K$ = 0.6).

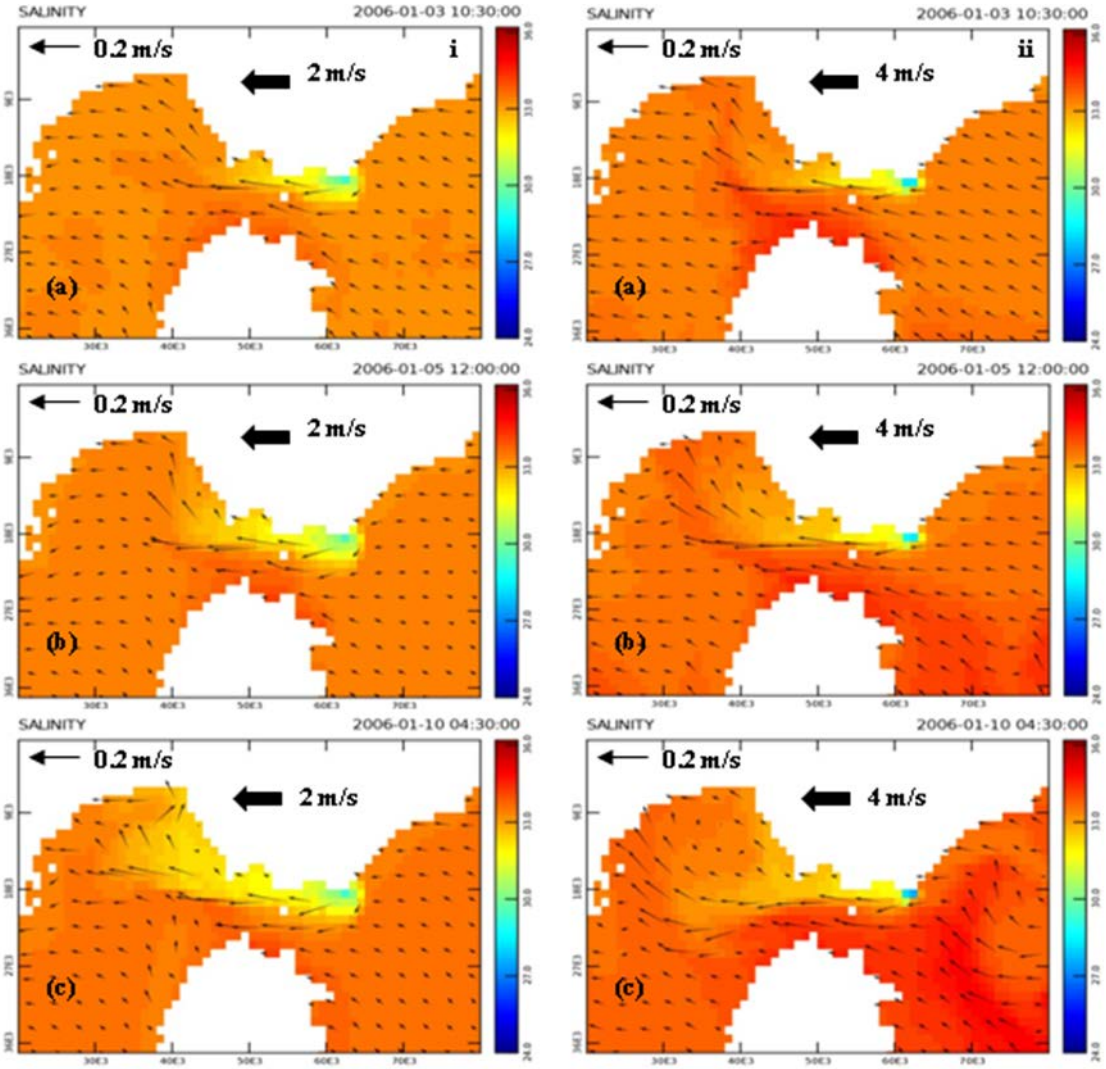


Figure 10. Nestos plume evolution with the introduction of easterly wind for R5 case (speed 2 m/s, left panel) and for R6 case (speed 4 m/s, right panel) during: (a) day 3, (b) day 5 and (c) day 10.

*River discharge influence*

The river discharge influence on the plume expansion was examined in simulation R7. This run was similar to R5 and the only difference was the increase of river runoff to 80 $m^3/s$. This kind of discharge is representing an occurrence of about 2% during the period 2006 - 2007, so it is a rare event. At $T$ = 0.4 days the outflowing freshwater developed an anticyclone, while the coastal current was formed at $T$ = 0.6 days. The anticyclone continued to grow, swirling significant amount of river water until day 6, having radius of 5 km (Fig. 11). Similar to R5 case, the plume maintained a westerly direction and squeezed to the coastline due to Ekman transport. The plume appeared more compact compared to the R5 case and during the fifth day it occupied the top 9 m of the water column at the mouth. Inside Thassos passage, the plume velocity reached 0.36 m/s, significantly higher than the R5 case (0.16 m/s). The plume entered Kavala Gulf and moved parallel to the eastern coastline, in a manner similar to R5 simulation. The classification parameters calculated from the results of the model showed that the plume remained subcritical, while its behavior is determined mainly by Coriolis force ($Fr$ = 0.44, $K$ = 1.92). However, the inertial Rossby radius measured from 2.2 km (R5) at 4.6 km, indicating the increase of the area where the inertial forces prevailed (Mestres et al. 2003). On the 5th day of the simulation the surface coverage of the plume was estimated at 220 $km^2$, while in R5 case it reached 185 $km^2$.

The detailed examination of salinity and velocity distributions were held at points P4 and P11 (Fig. 12). As the plume headed westwards, it arrived at P11 within $T$ = 0.75 days, i.e., 9.6 hours earlier compared to R5 case (Fig. 12a). From this time and until the end of the simulation this point continued to receive the plume water, causing an average salinity drop of about 1.5 psu for the entire simulation. The corresponding decrease for the R5 case was modeled at 0.6 psu. The wider range of salinity values in R7 simulation is once again attributed to the higher values of horizontal speed (Fig. 12b), which caused the acceleration of vertical mixing. As shown in Figure 12b, the plume arrival at P11 caused the increase of horizontal speed from about 0.08 m/s to 0.24 m/s, and subsequently up to 0.43 m/s. Keeping the wind speed and tidal range constant, the additional velocity inside the plume is only attributed to the river flow increase. Based on the simulation results, the gravitational wave speed $c$ inside the plume for the R7 case was doubled compared to the R5 case (0.02 and 0.01 $m/s^2$, respectively). Regarding point P4 which marks the entrance to Kavala Gulf, the plume arrived at $T$ = 0.9 days. As shown in Figure 12c, the average salinity from the time of plume arrival ($S$ = 31.0 psu) is lower than the corresponding salinity of P11 point ($S$= 31.5 psu) despite the fact that P4 is located 7 km to the west of P11. This incident demonstrates that the plume is compressed towards the continental coastline, due to Ekman transport.

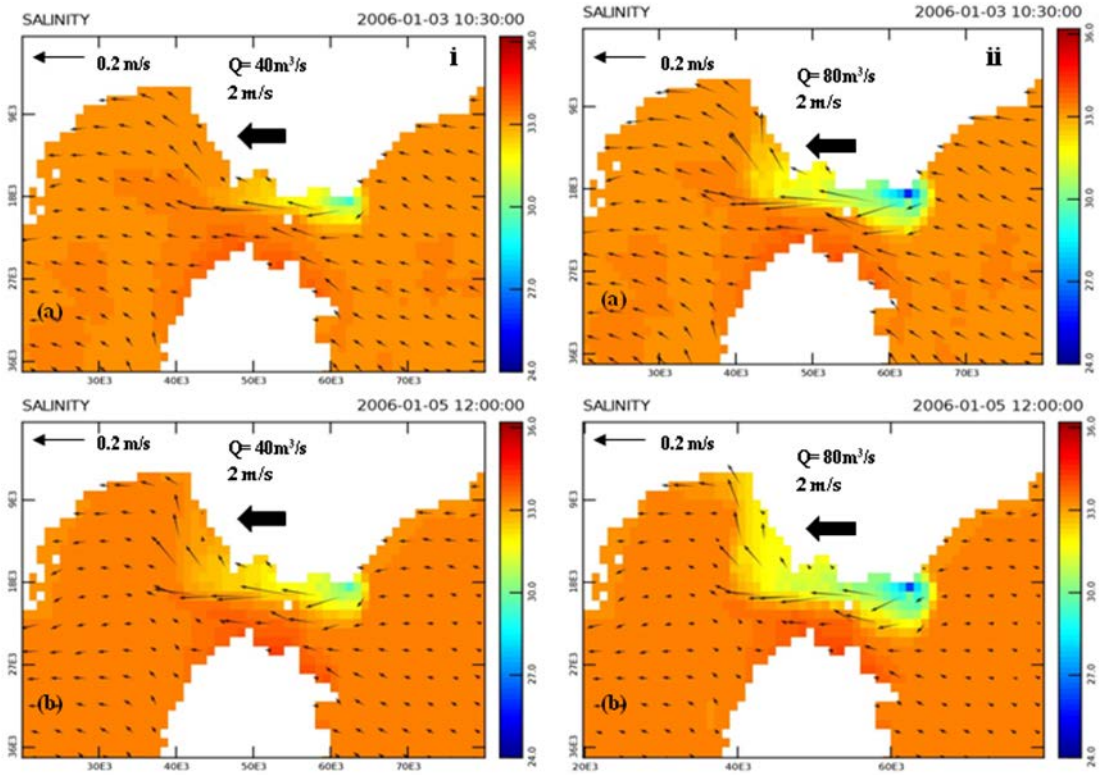


Figure 11. Nestos plume evolution with the introduction of easterly wind for R5 case (40 m3/s discharge, left panel) and for R7 case (80 m3/s discharge, right panel) during: (a) day 3 and (b) day 5.

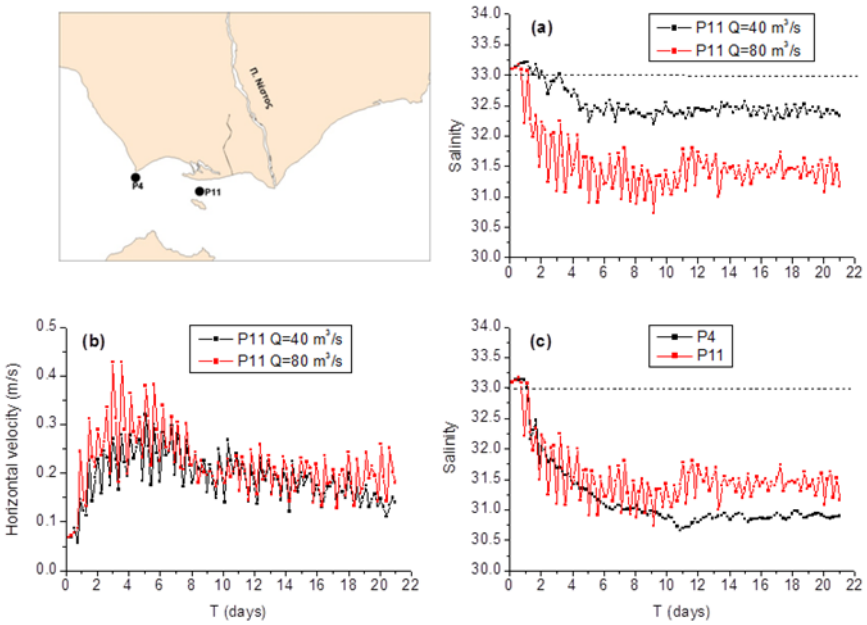


Figure 12. Temporal distribution of: (a) surface salinity, (b) horizontal velocity (positive values are indicating western movement) at P11 point for R5 and R7 cases and (c) surface salinity at points P11 and P4 for R7 simulation (80 m3/s discharge).

*Coastal morphology influence*

The morphology of the coastline upon the behavior of Nestos plume is investigated in this simulation. The previous chapters have shown the significant role of Thassos Passage in the western expansion of the plume, due to hydraulic conditions developed by its morphology. The degree of influence of the strait is determined by subtracting the island of Thassos (R9 case), thus creating a unified maritime zone westwards of the mouth. For this simulation, a northerly wind (0°) was applied having 2 m/s speed. The results of the simulation are compared with the R8 case, which includes Thassos Island. The plume evolution for both cases is illustrated in Figure 13. In case R8, the plume headed southwards, due to the combined effect of the initial momentum and wind direction, reaching a speed of 0.24 m/s, and immediately diverted westwards inside the strait. The speed of the plume in the strait ranged between 0.09 and 0.15 m/s, significantly higher than in the rest of the surface layer (0.05 – 0.11 m/s, Fig. 14) and entered Kavala Gulf after $T$ = 1.7 days. At time $T$ = 5 days, the plume was directed towards the center of the Gulf, and then turned to the southwest due to Ekman transport (Fig. 13b). The simulation also showed limited plume spreading along the eastern shoreline of the gulf on day 10. The speed of the plume increased over time due to the constant wind application and the morphology of the strait and reached 0.16 m/s on day 5 and up to 0.19 m/s on day 10 of the simulation (Fig. 14b and 14c).

In the case R9 (Thassos removal), the plume is directed primarily southwards and then turns to the southeast due to the combined effect of the Coriolis and the wind action. Compared to R8 case, this offshore spreading was found larger by 1 km, while the western coverage was 3 km shorter (Fig. 13a). The plume arrival at Kavala Gulf was delayed by 1.3 days, while during day 3 its speed was found lower between 0.04 and 0.09 m/s (Fig. 14a). On the 5th day the plume showed some similarities with the previous scenario, as its western expansion continues. This western deployment is, however, limited and estimated at 25 km from the mouth (30 km in case R8, Fig. 13b). The plume extended further southwards at a distance of 7 km from the mouth.

Regarding the classification parameters, both plumes were similar. The Froude number was found at 0.36 and 0.33 and Kelvin number at 2.2 and 2.6 for R8 and R9 cases, respectively. However, during day 5 the surface coverage in the R8 simulation was significantly larger than that in R9 (185 and 161 km$^2$, respectively). The major alternation between these cases inside

Kavala Gulf occurred from day 8. In the case of Thassos absence, the westward spreading stopped and two branches were created, the first running parallel to the eastern coast of the Gulf and the second to the southwest. The lower speed of the surface layer (Fig. 14c) and the gradual depth increase at the center of the Gulf directed the majority of the plume water northwards. In R8 case, the additional velocity, gained by the strait morphology, ejected the plume inside the Gulf; later it is deflected later southwestwards, due to Ekman transport. The significance of Thassos Passage to the transport of the plume is also examined by Sylaios et al. (2013). According to the same authors, the wind-induced residual flow directed mostly from northeast to southwest. Furthermore, the along-channel potential energy anomaly flux due to buoyancy input is once again directed westwards.

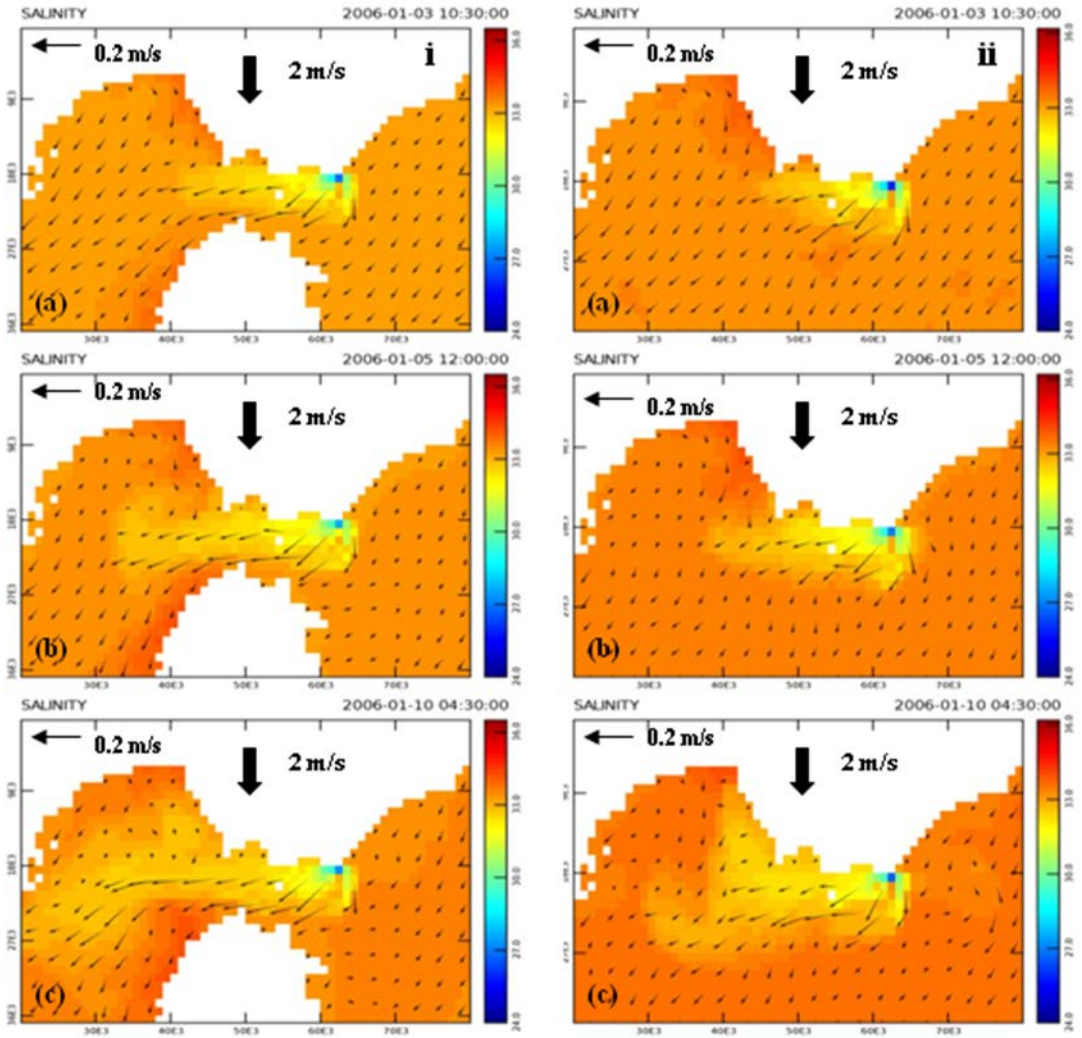


Figure 13. Nestos plume evolution with the introduction of northerly wind for R8 case (including Thassos, left panel) and for R9 case (Thassos removal, right panel) during: (a) day 3, (b) day 5 and (c) day 10.

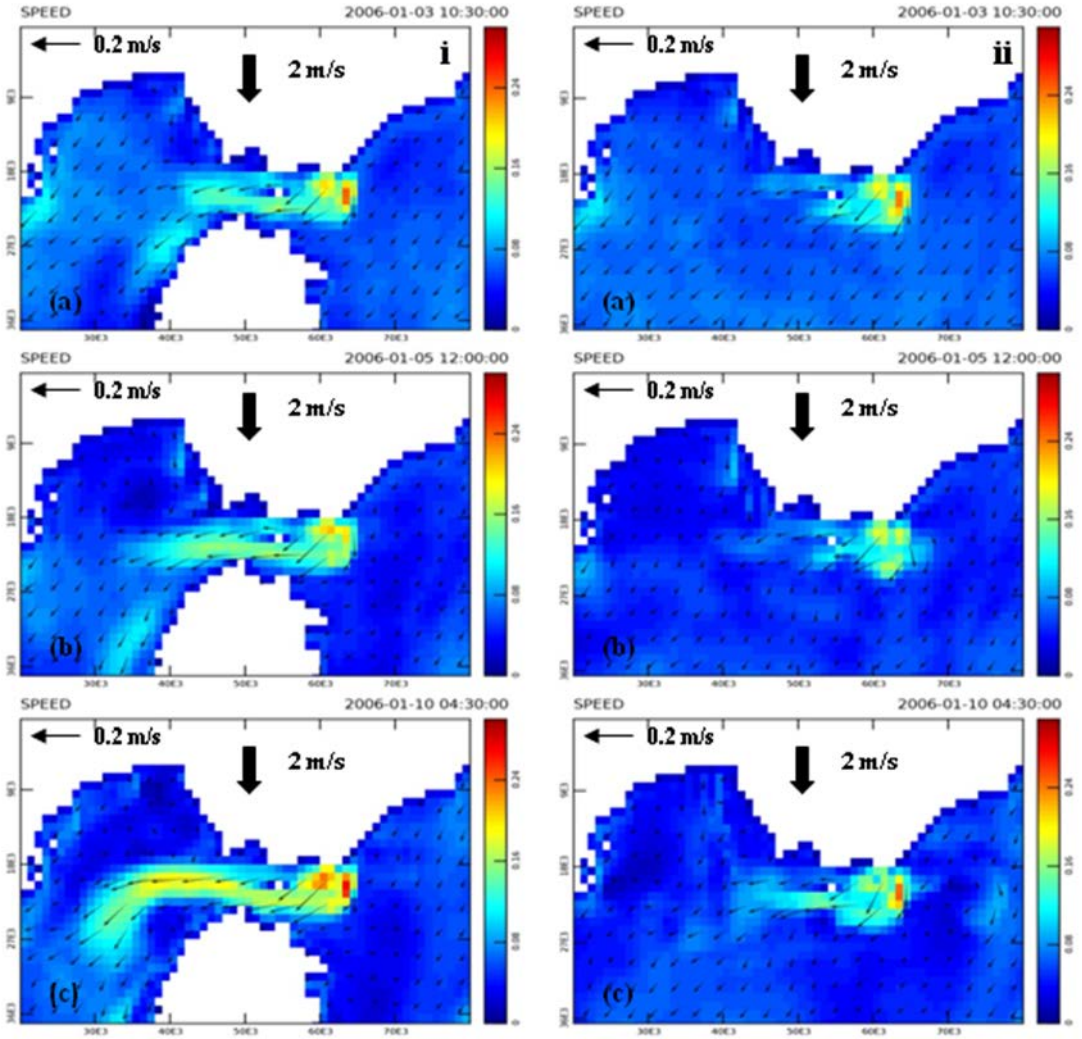


Figure 14. Horizontal velocity surface distribution for R8 case (including Thassos, left panel) and for R9 case (Thassos removal, right panel) during: (a) day 3, (b) day 5 and (c) day 10.

**Conclusions**

Properly verified mathematical models may reveal to a large extent the mechanisms of the external forcing that influence the growth rate, the size and shape of river plumes. In this study the application of a validated ELCOM model allowed the investigation of the degree of influence of various physical forcings upon Nestos River plume. Results showed that the behavior of Nestos plume is highly affected by the atmospheric forcing, while its size is determined mainly by the river discharge. The plume follows the direction of the wind having small clockwise deflection through Ekman transport. The wind velocity is important because it pushes the plume at distances from the mouth, while at the same time the mixing with the underlying seawater is accelerated as wind speed increases. However, under low wind conditions, the Coriolis force becomes more dominant. The general cyclonic circulation in the North Aegean Sea, the atmospheric forcing, and Coriolis force favor the western plume expansion. The results of the model showed that western spreading occurs under north to south-southeastern winds (0-170°), which have 65% occurrence during 2006-2007 period. The Thassos Passage also plays a crucial role in the western expansion and the shape and evolution of the plume, due to its narrowing. The surface waters within the strait gain extra speed and under high river discharge cases the plume enters Kavala Gulf. Tide has a secondary role on the plume behavior, due to the micro-tidal nature of the area.

**References**


Boskidis I., Gikas G.D., Sylaios G.K. and Tsihrintzis V.A., 2012. Hydrologic and water quality modeling of lower Nestos river basin. Water Resources Management, 26, 3023-3051.

Bricker J.D., Okabe I. and Nakayama A., 2006. Behavior of a small pulsed river plume in a strong tidal cross-flow in the Akashi Strait. Environmental Fluid Mechanics, 6, 203-225.

Casulli V. and Cheng R.T., 1992. Semi-implicit finite difference methods for three dimensional shallow water flow. International Journal for Numerical Methods in Fluids, 15, 629–648.

Chao S.Y. and Boicourt W.C., 1986. Onset of estuarine plumes. Journal of Physical Oceanography, 16, 2137-2149.

Chao S.Y., 1988a. River forced estuarine plumes. Journal of Physical Oceanography, 18, 72-88.

Fong D.M., 1998. Dynamics of freshwater plumes: observations and numerical modelling of the wind-forced response and alongshore freshwater transport. Ph.D. Thesis, MIT/WHOI Joint Program in Oceanography, Woods Hole.

Ganoulis J., Skoulikaris H. and Mognet J.M., 2008. Involving stakeholders in transboundary water resources management: The Mesta/Nestos 'HELP' basin. International Symposium 'HELP in action: Local Salutations to Global Water Problems Lessons from the South'. Emperor's Palace Johannesbourg, South Africa, 4-9 November 2007.

Garvine R.W., 1974. Physical features of the Connecticut River outflow during high discharge. Journal of Geophysical Research, 79 (6), 831–846.

Garvine R.W., 1981. Frontal jump conditions for models of shallow, buoyant surface layer hydrodynamics. Tellus, 33, 301–312.

Garvine R.W., 1982. A steady state model for buoyant surface plume hydrodynamics in coastal waters. Tellus, 34, 293–306.

Garvine R.W., 1987. Estuary plumes and fronts in shelf waters: a layer model. Journal of Physical Oceanography, 17, 1877-1896.

Garvine R.W., 1995. A dynamical system for classifying buoyant coastal discharges. Continental Shelf Research, 15, 1585-1596.

Gaston T.F., Schlacher T.A. and Conolly R.M., 2006. Flood discharges of a small river into open coastal waters: Plume traits and material fates. Estuarine, Coastal and Shelf Science, 69, 4-9.

Hetland R.D. and MacDonald D.G., 2008. Spreading in the near-field Merrimack River plume. Ocean Modeling, 21, 12–21.

Hodges B.R., 2000. Numerical Techniques in CWR-ELCOM (Code Release v.1). CWR Manuscript WP1422 BH, Centre for Water Research, University of Western Australia Publications, Perth.

Hodges B., Dallimore C., 2006. Estuary, Lake and Coastal Ocean Model:ELCOM, v2.2. Science manual. Centre for Water Research, University of Western Australia, Perth, Australia.

Horner-Devine A.R., Jay D.A., Orton P.M. and Spahn E.Y., 2009. A conceptual model of the strongly tidal Columbia River plume. Journal of Marine Systems, 78, 460-475.

Isari S., Fragopoulou N. and Somarakis S., 2008. Interannual viariability in horizontal patterns of larval fish assemblages in the northeastern Aegean Sea (Eastern Mediterranean) during early summer. Estuarine, Coastal and Shelf Science, 79, 607-619.

Kamidis N., Sylaios G. and Tsihrintzis V.A., 2011. Modeling the Nestos River plume dynamics using ELCOM. Desalination and Water Treatment, 33, 22-35.

Kourafalou V.H., Oey L.-Y., Wang J.D. and Lee T.N., 1996a. The fate of river discharge on the continental shelf: Part I. Modeling the river plume and the inner-shelf coastal current. Journal of Geophysical Research, 101 (C2), 3415–3434.

Kourafalou V.H., Lee T.N., Oey L. and Wang J.D., 1996b. The fate of river discharge on the continental shelf: Part 2. Transport of coastal low-salinity waters under realistic wind and tidal forcing. Journal of Geophysical Research, 101, 3435–3455.

Kourafalou V.H., 2001. River plume development in semi-enclosed Mediterranean regions: North Adriatic Sea and North Aegean Sea. Journal of Marine Systems, 30, 181-205.

Koutroumanidis T., Sylaios G., Zafeiriou E. and Tsihrintzis, V.A., 2009. Genetic modeling for the optimal forecasting of hydrologic time-series: Application in Nestos River. Journal of Hydrology, 368, 156-164.

Laval B., Imberger J., Hodges B.R. and Stocker R., 2003. Modeling circulation in lakes: spatial and temporal variations. Limnology and Oceanography, 48, 983–994.

Leonard B.P., 1991. The ultimate conservative difference scheme applied to unsteady one-dimensional advection. Computer Methods in Applied Mechanical Engineering, 88, 17–74.

Liu J.T., Chao S. and Hsu R.T., 2000. The influence of suspended sediments on the plume of a small mountainous river. Journal of Coastal Research, 16(2), 498-500.

Lykousis V., Chronis G., Tselepides A., Price N.B., Theocharis A., Siokou-Frangou I., Van Wambeke F., Danovaro R., Stavrakakis S., Duineveld G., Georgopoulos D., Ignatiades L., Souvermezoglou A. and Voutsinou-Taliadouri F., 2002. Major outputs of the recent multidisciplinary biochemical researches undertaken in the Aegean Sea. Journal of Marine Systems, 33-34, 313-334.

MacCready P., Banas N.S., Hickey B.M., Dever E.P. and Liu Y., 2009. A model study of tide- and wind-induced mixing in the Columbia River Estuary and plume. Continental Shelf Research, 29, 278-291.

Mestres M., Sierra J.P., Sánchez-Arcilla A., Del Rio J.G., Wolf T., Rodríguez A. and Oillon S., 2003. Modelling the Ebro River plume. Validation with field observations. Scientia Marina, 67, 379-391.

Petalas C., Pliakas F., Diamantis I. and Kallioras A., 2005. Development of an integrated conceptual model for the rational management of the transboundary Nestos River, Greece. Environmental Geology 48, 941-954.

Poulos S.E., Drakopoulos P.G. and Collins M.B., 1997. Seasonal variability in sea surface oceanographic conditions in the Aegean Sea (Eastern Mediterranean): an overview. Journal of Marine Systems, 13, 225-244.

Romero J.R., Antenucci J.P., Imberger J.,2004. One and three-dimensional biochemical simulations of two differing reservoirs. Ecological Modelling, 174, 143–160.

Sylaios G., Stamatis N., Kallianiotis A. and Vidoris P., 2005. Monitoring and assessment of land-based nutrient loadings, distributions and cycling within Kavala Gulf. Water Resources Management, 19, 713-735.

Sylaios G.K., Akratos C., Pissinaras V., Kamidis N. and Tsihrintzis V.A., 2008. 'TRITON': A monitoring station for wave climate, hydrodynamics and turbidity offshore Nestos River mouth, N. Greece. In: Proceedings of the 9th International Conference on Protection and Restoration of the Environment, Kefalonia, 2008.

Sylaios G., Kamidis N., Anastasiou S. and Tsihrintzis V.A., 2013. Hydrodynamic response of Thassos Passage (N. Aegean Sea) to Nestos River discharge and meteorological forcing. Continental Shelf Research, 59, 37-51.

Tanaka K., Michida Y., Komatsu T. and Ishigami K., 2009. Spreading of river water in Suruga Bay. Journal of Oceanography, 65, 165-177.

Ulses C., Grenz C., Marsaleix P., Schaaff E., Estournel C., Meulé S. and Pinazo C., 2005. Circulation in a semi-enclosed bay under influence of strong freshwater input. Journal of Marine Systems, 56, 113-132.

Yüce H., 1995. Northern Aegean water masses. Estuarine Coastal and Shelf Science, 41, 325-343.

Wiseman, W. and Garvine R.W., 1995. Plumes and coastal currents near large river mouths. Estuaries, 18 (3), 509–517.

Xing J. and Davies A.M., 1999. The effect of wind direction and mixing upon the spreading of a buoyant plume in a non-tidal regime. Continental Shelf Research, 19, 1437–1438.